Alan D. Freed
Ph.D.
Senior Research Engineer
ASME Fellow
e-mail: alan.d.freed@nasa.gov
Bio Sciences and Technology Branch, NASA's
John H. Glenn Research Center at Lewis Field,
21000 Brookpark Road, Cleveland, OH 44135
and Adjunct Staff, Department of Biomedical
Engineering, The Cleveland Clinic Foundation,
9500 Euclid, Avenue, Cleveland, OH 44195

Todd C. Doehring
Ph.D.
Research Associate
e-mail: doehrint@ccf.org
Department of Biomedical Engineering, ND-20,
Lerner Research Institute, The Cleveland Clinic
Foundation, 9500 Euclid Avenue,
Cleveland, OH 44195

Elastic Model for Crimped Collagen Fibrils

A physiologic constitutive expression is presented in algorithmic format for the nonlinear elastic response of wavy collagen fibrils found in soft connective tissues. The model is based on the observation that crimped fibrils in a fascicle have a three-dimensional structure at the micron scale that we approximate as a helical spring. The symmetry of this wave form allows the force/displacement relationship derived from Castigliano's theorem to be solved in closed form: all integrals become analytic. Model predictions are in good agreement with experimental observations for mitral-valve chordæ tendineæ.
[DOI: 10.1115/1.1934145]

1 Introduction

Soft passive tissues are multiconstituent materials that, from a load carrying point of view, are predominantly composed of two elastic substances (elastin and collagen) immersed in a hydrated proteoglycan gel (ground substance) [1]. The elastin network, unorganized collagen filaments of random orientation, and the hydrated gel collectively form a mixture (ground substance matrix) whose overall response is isotropic [2]. Organized collagen fibers, on the other hand, form fibrous networks that introduce strong anisotropic attributes into the tissue response [3].

The motivation for this investigation was a requirement that surfaced while developing an anisotropic constitutive model for soft tissues that accounts for the effect of fiber splay in an efficient manner, thereby making the overall model suitable for finite-element implementation. In this construction, both fiber stress $\sigma(\lambda)$ and fiber modulus $d\sigma(\lambda)/d\lambda$ are required as material inputs, with λ being fiber stretch.

The objective of this paper is to derive a material model of algebraic construction (efficient, no integrals) for the elastic response of fibrous, soft, connective tissues. It is desired that its parameters relate to measurable geometric features of collagen crimp. To keep the model simple, the response of a single crimped fiber is assumed to be representative of an ensemble of fibers: no effects from fiber/fiber crosslinks, fiber/matrix interactions, or fiber recruitment are considered in this study.

2 Collagen

Collagen molecules are built from polypeptide chains [2]. These molecules are synthesized within cells as a tropocollagen, and then secreted into the surrounding connective tissue through cell vesicles. The tropocollagen polymer has a triple-helix geometry whose length is about 285 nm and whose diameter is 1.4 nm. A single tropocollagen self-assembles with four other tropocollagen in the extracellular matrix at quarter-stagger intervals of 67 nm (D period) to form a microfibril whose diameter is about 3.5 nm [4]. Glycosaminoglycans (GAGs) serve as the cross-linking agent in this assembly process, with chemical attachments primarily located at the D-period banding sites. Microfibrils are gathered together via lateral and end-to-end aggregations to form subfibrils with a 10–20 nm diameter, which themselves aggregate to form fibrils with a 50–500 nm diameter [5]. The outcome is a slender, flexible fibril with fractal geometry. Fibrils are the fibrous entities observed in photographic images taken by scanning electron microscopes, like the image presented in Fig. 1.

Fibrils are assembled by the human body in a variety of ways to meet the varying needs of its soft tissues. Because the aspect ratio of a fibril is huge (2000–2500 to 1 [7]), it readily buckles under the internal restoring forces of the elastin matrix whenever a fibrous tissue is free from external load [8]. This rumpled configuration is known as crimp (see Fig. 1). Crimp occurs at the level of a fascicle—an aggregate of fibrils—which is the sixth tier in the collagen hierarchy [5]. Collagen fibers are assemblages of fibrils or fasciclæ, depending on the tissue; for example, chordæ tendineæ are "yarns" of fibrils (i.e., a fascicle), while tendons are "ropes" of fasciclæ. The wavy structure of crimp has a periodicity of between 10 and 100 μm, depending on the tissue. Tissues with shorter wavelengths tend to have greater extensibilities, as there seems to be less variability in crimp amplitude than crimp wavelength between the various tissues [6].

2.1 Collagen Mechanics. The response of collagen dominated tissues to external loads can be divided into three regions, as shown in Fig. 2. In the first region, called the toe region, collagen extends carrying load as if it were an uncoiling spring. No stretching at the micro-fibril level is observed; the D-spacing remains constant throughout the nonlinear (toe/heel) region [9].

As deformation leaves the toe region, passing through the heel in the stress/stretch curve, the response enters a nearly linear domain of substantial stiffness. Here the collagen fibrils have been stretched from their former wavy shape into a straightened configuration. Stretch arises from several mechanisms in the linear region. The D spacing at the microfibril level has been observed to extend from 67 to 69 nm, but this only contributes about 40% to the overall stretch [9]. Another possible mechanism for stretch is the deformation of mechanical linkages binding the various tiers in the collagen hierarchy; a folding-over and extension-of the GAG crosslinks [6]. The extent that this combined shear-lag/fluid-transport mechanism contributes to the overall elastic stiffness is unknown.

Fiber tearing generally occurs at the end of stretching in the linear region. Fibrils tear; they do not deform plastically, although

Contributed by the Bioengineering Division for publication In the JOURNAL OF BIOMECHANICAL ENGINEERING. Manuscript received: May 18, 2004. Revision received: February 1, 2005. Associate Editor: Jay D. Humphrey.

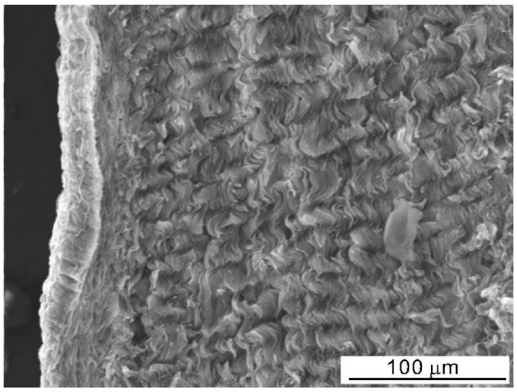

Fig. 1 Scanning electron microscopy (SEM) photograph of a cross-sectional cut of a chordæ tendineæ taken from a porcine mitral valve showing a three-dimensional (3D) undulating fiber structure. (Reproduced with permission from J. Liao [6].)

plasticity concepts have been applied to them [2]. Figure 2 represents the response of a single crimped fibril. A fiber is a collection of fibrils, wherein the failure of individual fibrils occur at different states producing a collective stress/strain response (beyond the heel region) whose eventual failure is more gradual and graceful than that of an individual fibril. In this regard, a fiber model based on recruitment will be required to correctly model tearing, which we do not consider herein.

The elastic modulus of a collagen molecule is about 3 GPa, while a single collagen fibril has an elastic modulus of around 400 MPa [10]. Both have linear stress/strain responses. The existence of crimp in aggregates of fibrils is the primary cause of the characteristic nonlinear response that is so prevalent in soft-tissue data. The nonlinear effect that crimp has on mechanical response has been known for nearly a century [11]. Crimped collagen tissues typically have an elastic modulus in the upper 10s to lower 100s of megapascal when measured in the linear region. The elastic modulus therefore appears to decrease as lower-level assemblages aggregate into higher-level architectures in the collagen-fiber hierarchy [10]; however, there are conflicting data in this regard [12].

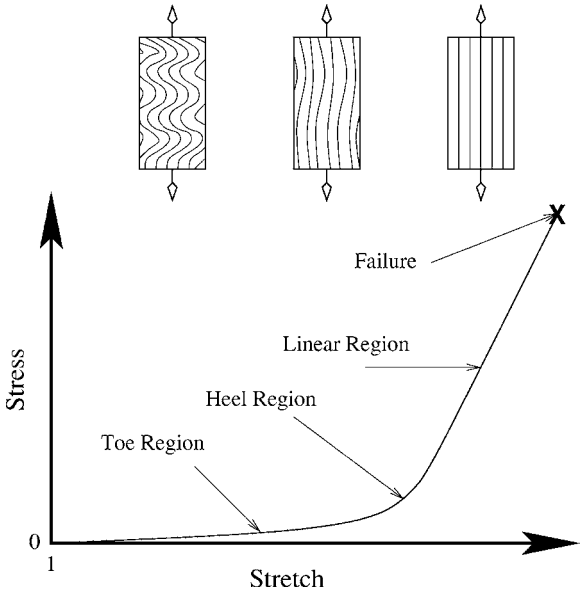

Fig. 2 A schematic of the stress/stretch response of collagenous tissues and how their wavy structures vary with deformation

2.2 Collagen Models. Material models for collagen generally belong to one of two classes: phenomenological or structural. Both micro- and macrovariants belonging to these material classes have been constructed.

Phenomenological models have material parameters with no direct physical or morphological basis. The exponential function is most commonly employed in such descriptions of collagen [13]. Power-law functions have also been used with good success in this regard [14].

Structural models have physiologic parameters. There are predominantly two types of structural crimp models that have been reported on in the literature. Both consider two-dimensional wave forms for describing crimp. They are outgrowths from two distinct camps of thought: one being that crimp has a fairly smooth planar wave form like a sinusoid, and the other being that crimp has a more jagged planar wave form like a sawtooth. Both perspectives base their hypothesis upon microscopic evidence.

Comninou and Yannas [15] and Lanir [1] derived constitutive formulæ for collagen fibers from a sinusoidal wave form for crimp, as advocated by Dale et al. [16]. Both models have been shown to correlate experimental data reasonably well. Lanir's model includes a fiber/matrix (i.e., collagen/elastin) interaction effect.

Zig-zag models based on kinematic linkages with rigid hinges and flexible links [17], with flexible hinges and rigid links [18], and with flexible hinges and flexible links [19] constitute a second class of assumed collagen fiber wave forms. They correlate data with varying degrees of realism.

In contrast, our collagen model assumes a smooth 3D wave form for describing crimp; specifically, we employ a cylindrical helix. Evans and Barbenel [20] and Yahia and Drouin [21] have both reported that planar and helical crimp patterns exist. The wave form shape depends on both tissue and location. Lerch [22] was the first to describe the geometric features of crimp, and this he did using the geometry of a cylindrical helix for representing crimp wave form. Beskos and Jenkins [23] were the first, and apparently the only ones (other than us) to derive a constitutive expression for crimped collagen based on a cylindrical helix for the wave form. However, their model predicts an infinite stiffness at full extension due to an assumption of fiber in-extensibility, which is not realistic.

In measurements of crimp angle versus strain, Dale et al. [16] observed actual tissue behavior to be bounded between curves from an extending sine wave (from below) and an extending cylindrical helix (from above). In this paper, we derive a physiologically based constitutive expression (at the micron scale) characteristic of this helical bound.

Lanir [24] proposed assembling an aggregate of microconstitutive fibril models, each oriented in a different direction, whose collective response is obtained by averaging via some probability distribution function. The outcome is a physically based, homogenized, macroconstitutive equation appropriate for tissue modeling. Herein, we derive a physically based material model of a simpler algebraic construction that is likely to be more suitable for use in a finite-element setting.

Many passive soft tissues act as tethers, transmitting loads from one attachment point to another in a one-dimensional manner; for example: tendons, ligaments, and the chordæ tendineæ of heart valves. The derivation of our elastic model for collagen is based upon this observation, and upon the following set of constitutive assumptions:

(1) The wave form used to represent crimp is that of a cylindrical helix which extends into a straightened configuration in the linear region of deformation
(2) The only load carried by a crimped fibril is an axial force acting along the centerline of the helix, which is consistent with spring theory, torsion springs withstanding [25]

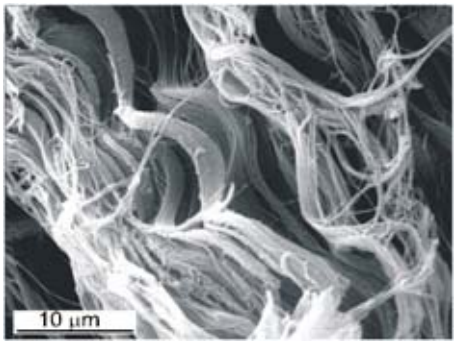

Fig. 3 SEM photograph showing the helical nature of crimped collagen fibrils in chordæ tendineæ taken from a porcine mitral valve. (Reproduced with permission from J. Liao [6].)

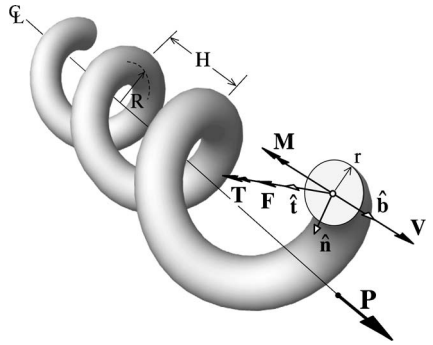

Fig. 4 Diagram of how force P acting along the centerline of a helix is transferred to forces F and V and moments M and T that act along the backbone of the helix

(3) Microstructurally, the chord of a helix deforms elastically, in accordance with linear (infinitesimal deformation) theory. Macrostructurally, the helical fiber deforms in accordance with finite-deformation theory
(4) No interactions are considered between neighboring helices (e.g., there is no fiber recruitment [26] or out-of-phase wave pattern [27]), or between a fibril and the ground substance matrix that it resides in [1]
(5) The molecular dimensions along the backbone of a helix remain fixed when loaded in the nonlinear region; only when loaded into the linear region are these dimensions allowed to change [9], and incompressibility is imposed

By exploiting the geometry of a cylindrical helix, we are able to derive a physiologically based material model that is representative of the nonlinear stress/strain response exhibited by soft collagenous tissues. An advantage of adopting a cylindrical helix for the wave form of crimp is that the symmetry in its geometry mitigates the need to integrate along the helical axis, thereby producing an algebraic constitutive expression that is free of calculus operators.

3 Geometric Model for Collagen Fibrils in a Fascicle

Figure 3 presents a close-up of Fig. 1, where one observes that collagen fibrils have a 3D helical shape in a fascicle free from external traction, thereby providing experimental justification for assumption (1) earlier. Three different protocols were followed for SEM specimen preparation by Liao [6], all resulting in images of crimped collagen fibrils that undulate in 3D space.

3.1 Geometry of a Cylindrical Helix. Consider a fibril in a reference frame that is free from external traction, and assume that this fibril takes on the shape of a cylindrical helix. Let the height (or wavelength) of this helix be denoted by H, which has a typical value ranging between 10 and 100 μm, and let its radius (or amplitude) be given by R, which has a typical value ranging between 1 and 10 μm [4]. Consequently, the chord length L of one helical revolution is determined to be $L=(4\pi^2R^2+H^2)^{1/2}$—a parameter that we shall assume remains fixed throughout deformation in the toe and heel regions, in accordance with assumption (5) earlier. Furthermore, let the radius of this fibril be denoted by r—another parameter that we assume remains fixed, but whose value can vary between 50 and 500 nm depending on age, tissue, and location within the tissue [4]. When modeling a particular tissue, the three physiologic parameters H, R, and r represent statistical averages taken over the volume.

A cylindrical-polar coordinate system was employed by Ancker and Goodier [25] in their classic study of helical springs, and by Beskos and Jenkins [23] in the development of their collagen model. We, on the other hand, adopt the coordinate system of differential geometry, where the geometry of any curve in 3D space can be described by an orthogonal triad of unit base vectors, which for a cylindrical helix is given by [[28], p. 27]

$$\hat{\mathbf{t}} = \omega(-R\sin\omega s, R\cos\omega s, H)$$

$$\hat{\mathbf{n}} = (-\cos\omega s, -\sin\omega s, 0)$$

$$\hat{\mathbf{b}} = \omega(H\sin\omega s, -H\cos\omega s, R)$$

wherein $\hat{\mathbf{t}}$ is the tangent vector, $\hat{\mathbf{n}}$ is the normal vector, and $\hat{\mathbf{b}}$ is the binormal vector. Parameter s designates a location along the curve, while $\omega=(R^2+H^2)^{-1/2}$. Curvature κ and torsion τ (properties of curves in space) are equal in a helix, with $1/\kappa$ being the radius of curvature. For a cylindrical helix, $\kappa=R/(R^2+H^2)$ with $R>0$.

3.2 Extension of a Cylindrical Helix. Figure 4 presents a schematic of how a helical collagen fibril is considered to carry load. A force $\mathbf{P}=(0,0,P)$ is taken to act along the centerline of the helix in the 3 direction, in accordance with assumptions (2) and (4). Constructing a representative free-body diagram, this load can be translated out to the mean radius R of the helix, thereby producing normal $\mathbf{F}$ and shearing $\mathbf{V}$ forces that act on the face of the helix in directions $\hat{\mathbf{t}}$ and $\hat{\mathbf{b}}$, respectively, such that

$$\mathbf{F} = (\mathbf{P}\cdot\hat{\mathbf{t}})\hat{\mathbf{t}} = F\hat{\mathbf{t}}, \quad F = PH/\sqrt{R^2+H^2}$$

$$\mathbf{V} = (\mathbf{P}\cdot\hat{\mathbf{b}})\hat{\mathbf{b}} = V\hat{\mathbf{b}}, \quad V = PR/\sqrt{R^2+H^2} \tag{1}$$

while $\mathbf{P}\cdot\hat{\mathbf{n}}=0$. The act of moving $\mathbf{P}$ to the backbone of the helix also produces a bending moment $\mathbf{M}$ and a torque $\mathbf{T}$ that are quantified by

$$\mathbf{M} = R\hat{\mathbf{n}}\times F\hat{\mathbf{t}} = -RF\hat{\mathbf{b}} = -M\hat{\mathbf{b}}, \quad M = PRH/\sqrt{R^2+H^2}$$

$$\mathbf{T} = R\hat{\mathbf{n}}\times V\hat{\mathbf{b}} = RV\hat{\mathbf{t}} = T\hat{\mathbf{t}}, \quad T = PR^2/\sqrt{R^2+H^2}. \tag{2}$$

Scalars P, F, V, M, and T are the magnitudes of vectors $\mathbf{P}$, $\mathbf{F}$, $\mathbf{V}$, $\mathbf{M}$, and $\mathbf{T}$, respectively.

To illustrate the process, let us first consider the case of a straight filament whose linear-elastic strain energy is $U=1/2\int\sigma\epsilon dV$, wherein σ is stress, ϵ is strain, and V is volume. The total strain energy contained within such a filament is therefore $U_F=F^2L/2AE_f$, where F is the applied force, L is the length, $A=\pi r^2$ is the cross-sectional area, and E_f is the elastic modulus of the filament. An application of Castigliano's theorem [[29], pp. 133–136] leads to the following force/displacement relation

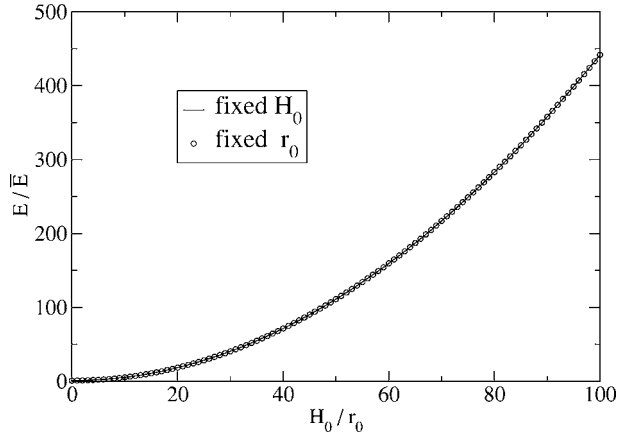

Fig. 5 Plots of crimp wavelength H_0 normalized by fibril radius r_0 (where in one curve H_0 varies, and in the other curve r_0 varies) vs the elastic modulus E normalized by the secant modulus $\bar{E}$ evaluated at the transition between heel and linear regions

$$\Delta L = \frac{\partial U_F}{\partial F} \quad \text{therefore} \quad F = K_f \frac{\Delta L}{L} \quad \text{where} \quad K_f = AE_f$$

where $\Delta L = L - L_0$ is the change in length, and K_f is the filament stiffness.

For a helix, adopting assumption (3), one must add to the earlier strain energy for extension U_F, strain energies for shear $U_V = 20V^2L/9AG_f$, bending $U_M = M^2L/2IE_f$, and torsion $U_T = T^2L/2JG_f$, which are derived in the appendix, wherein $I = (1/4)\pi r^4$ and $J = (1/2)\pi r^4$ are the moment and polar-moment of inertia, respectively, with G_f denoting the shear modulus of the filament, which we take to be $G_f = E_f/3$ in accordance with the incompressibility constraint of assumption (5). Another application of Castigliano's theorem, this time using Eqs. (1) and (2), leads to

$$\Delta H = \frac{\partial (U_F + U_V + U_M + U_T)}{\partial P} \tag{3a}$$

therefore

$$P = K\frac{\Delta H}{H} \text{ where } K = K_f \frac{R^2 + H^2}{LH[1 + 4R^2/r^2 + 6(20/9 + R^2/r^2)R^2/H^2]} \tag{3b}$$

with K being the elastic stiffness of a helical spring, which is proportional to the elastic stiffness K_f of a straightened filament. The first term in the parentheses of the denominator arises from stretching, the second term from bending, the third term from shearing, and the fourth term from twisting. All four energies are needed to obtain realistic behavior from the ensuing constitutive formula. It is the symmetry of a cylindrical helix along its axis that leads to an algebraic equation for stiffness (instead of an integral equation), which adds great utility to the resulting model.

Because the cross-sectional area $A = A_0$ of a helical coil is constant throughout the nonlinear region of its stress/strain response (a consequence of assumption (5)), Castigliano's theorem, via Eq. (3*b*), leads to a constitutive description whereby (Cauchy) stress $\sigma = \lambda P/A_0$, in some averaged sense, is proportional to (linear) strain $\epsilon = \lambda - 1 = (H - H_0)/H_0$, with the proportionality being a nonlinear function of stretch $\lambda = H/H_0$.

Our helical model for collagen appears to have three, independent, geometric parameters (viz., H_0, R_0, and r_0, which are the initial values for H, R, and r) but, in fact, there are only two. This is demonstrated in Fig. 5, where two different curves for H_0/r_0 are plotted against a normalized stiffness $E/\bar{E}$, wherein E is the elastic modulus of the linear region, and $\bar{E}$ is that secant modulus belonging to the point of transition between the heel and linear regions. In one curve, H_0 is held constant and r_0 is varied, while in the other curve, r_0 is held constant and H_0 is varied. The two curves are identical. Consequently, one is free to choose the dimensionless ratios H_0/r_0 and R_0/r_0 as representing the independent variables. These are physical parameters that can be measured by independent means, like a SEM photograph.

Linear beam theory was used in the derivation of Eq. (3*b*) as an approximation. We also employed the Winkler–Bach flexure formula from curved beam theory [[30], p. 142] and found that the additional effects due to curvature are negligible for helical geometries representative of crimp.

3.3 Constitutive Algorithm. Instead of writing a single formula for quantifying the stress/strain response of our constitutive model, with defining terms scattered throughout the text, it is useful to present our model in a concise algorithmic format written in terms of pseudo code, see algorithm (1). Given some axial stretch λ acting along a fiber, the algorithm returns the Cauchy stress σ carried by that fiber. To accomplish this objective, two normalizing parameters, $\bar{\lambda}$ and $\bar{E}$ (the former being a stretch and the latter being a secant modulus, both defined at the transition point between the heel and linear regions), and one scaling parameter ξ extracted from Eq. (3*b*) (whose product with $\bar{E}$ gives the secant modulus at any stretch λ with $\xi(\bar{\lambda}) = 1$) have been introduced. Four material constants need to be specified: H_0/r_0, R_0/r_0, E, and λ_u; three if fiber failure is ignored. Of these, the stretch at failure λ_u and the elastic modulus E (over the linear region) can be obtained directly from an experimental stress/strain curve. Acquiring the remaining two parameters, H_0/r_0 and R_0/r_0, is a more arduous task that can be facilitated through an optimization exercise.

Stretch $\lambda = H/H_0$ at the transition between heel and linear regions, denoted as $\bar{\lambda}$, is defined by

$$\bar{\lambda} = \frac{L}{H_0} = \frac{L_0}{H_0} = \frac{(4\pi^2 R_0^2 + H_0^2)^{1/2}}{H_0}.$$

The fact that chord length L remains fixed over the nonlinear region of deformation (viz., $L = L_0$ whenever $H < L_0$, or equivalently, whenever $R > 0$) is a direct consequence of assumptions (3) and (5). This constraint implies that stiffness only depends on geometry (it is independent of force), and as such, a simple constitutive expression follows.

The derivation of the secant modulus $\bar{E}$ is more tedious. The basic idea is to force the stress/strain response to be continuous and differentiable across the transition point between its nonlinear and linear regions. In the nonlinear region, where $\lambda \leqslant \bar{\lambda}$, the constitutive response is given by Eq. (3), which can be rewritten in terms of stress as $\sigma = \xi E_f(\lambda - 1)$, with ξ being as defined in Algorithm 1. In the linear region, where $\bar{\lambda} \leqslant \lambda$, stress has the linear construction $\sigma = \bar{E}(\bar{\lambda} - 1) + E(\lambda/\bar{\lambda} - 1)$, with the first term quantifying stress at the transition point $\lambda = \bar{\lambda}$, while the second term accounts for any additional stress where $\epsilon_{\text{additional}} = \Delta\ell/\ell_{\text{ref}} = (\ell - \ell_{\text{ref}})/\ell_{\text{ref}} = (\lambda\ell_0 - \bar{\lambda}\ell_0)/\bar{\lambda}\ell_0 = \lambda/\bar{\lambda} - 1$. In this second term, $\bar{\lambda}$ serves as a reference state from which additional straining is computed. Recalling that $\xi(\bar{\lambda}) = 1$, continuity of stress σ across the junction $\lambda = \bar{\lambda}$ implies that $E_f = \bar{E}$, while continuity of modulus $d\sigma/d\lambda$ across this same junction leads to the formula for secant modulus $\bar{E}$ that is listed in Algorithm 1.

Algorithm 1. *Given H_0/r_0, R_0/r_0, E, and λ_u, where H_0 is the initial wavelength of crimp, R_0 is the initial amplitude of crimp, r_0 is the initial fibril radius, E is the elastic modulus of the fiber in the linear region, and λ_u is its ultimate stretch, then*:

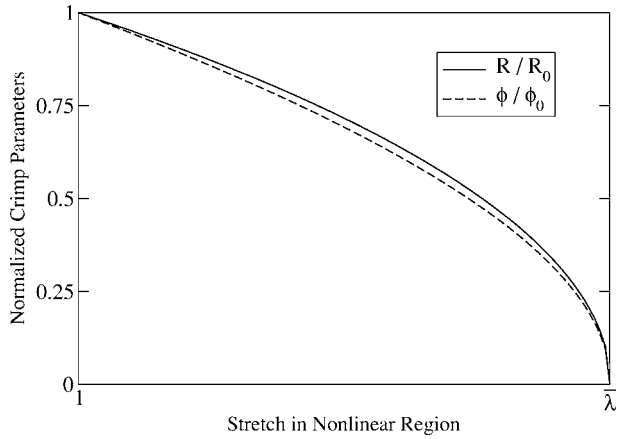

Fig. 6 Plots of the amplitude R and angle of pitch ϕ of crimp (normalized by their initial values R_0 and ϕ_0) vs stretch λ over the toe and heel regions

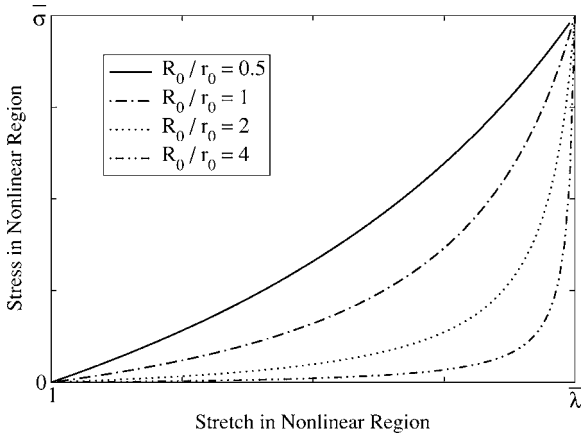

Fig. 7 Dependence of Algorithm 1 on parameter R_0/r_0, where $\bar{\lambda}$ and $\bar{\sigma}=\bar{E}(\bar{\lambda}-1)$ are values for stretch and stress at the transition point between linear and nonlinear behaviors. The linear region, where $\lambda>\bar{\lambda}$, is not shown.

Set $r_0=1$ *so that* $H_0 \equiv H_0/r_0$ and $R_0 \equiv R_0/r_0$.
Compute constant parameters:
$L_0=[(2\pi R_0)^2+H_0^2]^{1/2}$,
$\bar{\lambda}=L_0/H_0<\lambda_u$,
$\bar{E}=EH_0^2/L_0\{H_0+[1+37/6\pi^2+2(L_0/\pi r_0)^2](L_0-H_0)\}$.
If $\lambda \leqslant \bar{\lambda}$, *then*
(Yes, compressive stretches, i.e., $0<\lambda<1$, are allowed.)
$H=\lambda H_0$,
$R=(L_0^2-H^2)^{1/2}/2\pi$,
$\xi=(R^2/H^2)/\{L_0H[1+4R^2/r_0^2+6(20/9+R^2/r_0^2)R^2/H^2]\}$,
$\sigma=\xi\bar{E}(\lambda-1)$.
Else If $\bar{\lambda} \leqslant \lambda \leqslant \lambda_u$. *Then*
$\sigma=\bar{E}(\bar{\lambda}-1)+E(\lambda/\bar{\lambda}-1)$
Else (Fibril failure)
$\sigma=0$.
Return σ.

4 Discussion

A physiological model for collagen tensile behavior can be useful for elucidating structure-function relationships, and for assessing the mechanical behavior of tissues. The work presented in this paper provides a theoretical framework for representing collagen crimp based on the geometry of a cylindrical helix. We chose this helix geometry because recent morphological evidence indicates a helical structure for crimped collagen [6]. Indeed, helix-type structures are common in biological materials, e.g., DNA. Hence, the helix model developed herein may be useful in studies for a variety of biological materials.

Unlike classical spring theory, where the ratio of radii ($r/R<0.25$) and the angle of pitch ($\phi=\tan^{-1} H/4R<15°$) of a helix are constrained so that the spring stiffness remains approximately linear with deformation [25], the physics of crimped collagen requires the helix to stretch straight. A plot of changes in the amplitude R and angle of pitch ϕ over the toe and heel regions, whose responses are almost identical, is presented in Fig. 6; consequently, these measures can be used interchangeably.

There are two geometric parameters present in Algorithm 1, viz., H_0/r_0 and R_0/r_0. Of these, parameter R_0/r_0 has the greater influence on overall shape. This is illustrated in Figs. 7 and 8. Parameter R_0/r_0 controls the depth of the belly in the nonlinear region, i.e., the toe region, while parameter H_0/r_0 has a modest affect on the shape of the heel region, translating the heel along the abscissa. The fixed parameters were: $E=50$ MPa for both figures, $H_0/r_0=20$ for Fig. 7, and $R_0/r_0=2$ for Fig. 8.

The ability of Algorithm 1 to fit experimental data is demonstrated in Fig. 9. The data presented therein are from five chordæ tendineæ taken from porcine mitral valves. The experiments were done in a servohydraulic testing system using the protocol described in Ref. [31]. The cross-sectional areas and gage lengths of these five specimens were measured in their unloaded state. They were gripped using sinusoidal clamps, and immersed in a temperature controlled (37 °C) saline bath. An uniaxial ramp displacement (10 mm/s) was applied, and the resulting loads were recorded. Stretch was computed from the grip-to-grip displacement, while stress was computed from the measured load divided by the current cross-sectional area, assuming constant volume.

The helical model parameters H_0/r_0, R_0/r_0, and E were estimated using the direct-fit method described in Ref. [14]. The direct-fit method uses a grid-based global optimization approach to fit the model to the actual point-wise stress/stretch data. A single model fit was done using the data from all five specimens grouped together. Gage lengths were originally computed using an established protocol [32]. Because of the difficulty of assigning an accurate gage length to soft-tissue experiments, these original lengths were manually adjusted (by <0.5%, after applying the protocol of Ref. [32]) so that the linear portions of the stress/

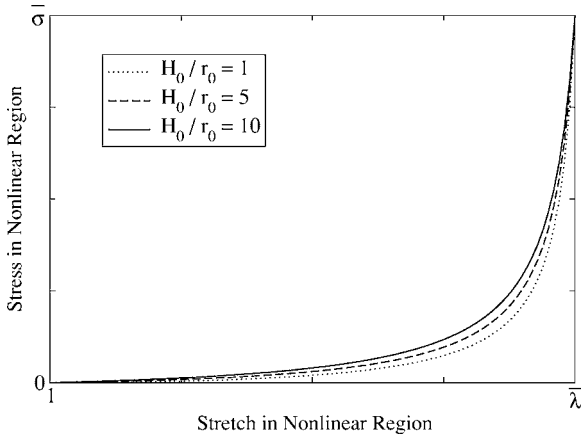

Fig. 8 Dependence of Algorithm 1 on parameter H_0/r_0, where $\bar{\lambda}$ and $\bar{\sigma}=\bar{E}(\bar{\lambda}-1)$ are values for stretch and stress at the transition point between linear and nonlinear behaviors. The linear region, where $\lambda>\bar{\lambda}$, is not shown.

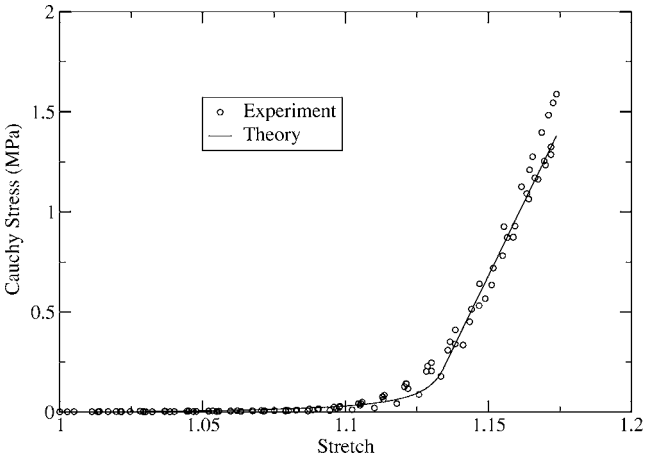

Fig. 9 A fit of the helix model to data taken from five, porcine, mitral-value, chordæ-tendineæ specimens

stretch curves came into good alignment. The resulting optimal model constants were: $H_0/r_0=22.5$, $R_0/r_0=1.92$, and $E=33.3$ MPa; resulting in the following parameters: $\bar{\lambda}=1.133$ and $\bar{E}=1.55$ MPa; with a dimensionless, residual, sum-of-squares error of 0.017, where $error=\Sigma_{n=1}^{N}[(\sigma_n-\sigma_n^{\exp})^2]^{1/2}/N\max_{n=1}^{N}|\sigma_n^{\exp}|$ with N being the total number of data points fit: in Fig. 9, N was 114. Values for the geometric parameters H_0/r_0 and R_0/r_0 are representative of reality, see Fig. 3. Recall that H_0 is the wavelength of a single crimped coil in a typical collagen fibril, R_0 is its amplitude, and r_0 is the fibril radius, see Fig. 4. These parameters have nothing to do with the fibril aspect ratio, mentioned in the Introduction, which is a different geometric property of collagen that this model does not take into consideration.

The low residual error obtained indicates that our helical model fits the data well, particularly in the toe region. The model fit is not as good in the heel region, however, having a stronger curvature and a more abrupt transition between the toe and linear regions than is otherwise apparent in the data. Additionally, in the linear region, the data tend to retain a small amount of curvature that is not represented by the model. These behaviors may be able to be accounted for by including fiber recruitment, which would tend to soften the curvature as fibers are gradually stretched. Including recruitment is beyond the scope of this work.

We were encouraged to find that the resulting optimal parameters for our relatively simple helical model corresponded well to the measured wavelengths and amplitudes of crimp observed in optical and SEM images of the chordæ. This further supports the hypothesis that a cylindrical helix representation may be representative of the actual tissue microstructure. Further applications to tensile testing of specimens with different crimp patterns (e.g., pericardium, rat-tail tendon, etc.) are needed to investigate possible relationships between model parameters and tissue microstructure.

Unlike other collagen fiber models, our model permits compressive states—a helical spring can compress. These states are very soft, and as such, carry negligible load. The real advantage of permitting compressive states is that they will likely add stability to numeric algorithms used in applications like finite elements.

Like the collagen model of Hurschler et al. [33], our model accounts for failure. Fibril failure is represented in a boolean manner. Fiber failure, to be correctly modeled, would need to be an integral sum over all fibrils in a fiber, as in fiber recruitment theory.

Acknowledgments

The authors take this opportunity to thank Dr. Daniel Einstein, Dr. Jun Liao, and Dr. Ivan Vesely for many delightful discussions on this and related topics. Constructive criticism from the anonymous reviewers is also greatfully acknowledged. Funding for ADF came from the US DoD (DAMD17-01-1-0673) to the Cleveland Clinic, Dr. Ivan Vesley (PI), conducted under Space Act Agreement SAA3-516. Funding for T.C.D. came from the US NIH (NHLBI HL 72598). This paper is dedicated to Prof. Bela I. Sandor on the occasion of his 70th birthday.

Appendix: Strain Energy Functions, $U=(1/2)\int \sigma\epsilon dV$

The geometry is that of a cylindrical rod with radius r, length L, elastic modulus E, and shear modulus G. The cross-sectional area is $A=\pi r^2$, the moment of inertia is $I=(1/4)\pi r^4$, and the polar moment of inertia is $J=(1/2)\pi r^4$. Any standard textbook in strength of materials can serve as a reference, e.g., Ref. [34].

(A) Axial force, F

$$U_F=\frac{1}{2}\int_0^L\int_{-r}^{r}\int_{-\sqrt{r^2-y^2}}^{\sqrt{r^2-y^2}}\frac{F}{A}\frac{F}{AE}dxdydz=\frac{F^2L}{2AE}$$

(B) Shear force, V

$$Q=\int_y^r\int_{-\sqrt{r^2-y^2}}^{\sqrt{r^2-y^2}}ydxdy=\frac{2}{3}(r^2-y^2)^{3/2}$$

$$U_V=\frac{1}{2}\int_0^L\int_{-r}^{r}\int_{-\sqrt{r^2-y^2}}^{\sqrt{r^2-y^2}}\frac{VQ}{Ix}\frac{VQ}{IxG}dxdydz=\frac{5V^2Lr^2}{9IG}=\frac{20V^2L}{9AG}$$

(C) Bending moment, M

$$U_M=\frac{1}{2}\int_0^L\int_{-r}^{r}\int_{-\sqrt{r^2-y^2}}^{\sqrt{r^2-y^2}}\frac{Mx}{I}\frac{Mx}{IE}dxdydz=\frac{M^2L}{2IE}$$

(D) Torque, T

$$U_T=\frac{1}{2}\int_0^L\int_0^{2\pi}\int_0^r\frac{Tr}{J}\frac{Tr}{JG}rdrd\theta dz=\frac{T^2L}{2JG}$$

References

[1] Lanir, Y., 1978, "Structure-Strength Relations in Mammalian Tendon," Biophys. J., **24**, pp. 541–554.
[2] Viidik, A., 1973, "Functional Properties of Collagenous Tissues," Int. Rev. Connect Tissue Res., **6**, pp. 127–215.
[3] Humphrey, J. D., 2002, "Continuum Biomechanics of Soft Biological Tissues," Proc. R. Soc. London, Ser. A, **459**, pp. 3–46.
[4] Nimni, M. E., and Harkness, R. D., 1988, "Molecular Structure and Functions of Collagen," in: *Collagen*, M. E. Nimni, ed., CRC Press, Boca Raton, Vol. I, Chap. 1, pp. 1–77.
[5] Kastelic, J., Galeski, A., and Baer, E., 1978, "The Multicomposite Structure of Tendon," Connect. Tissue Res., **6**, pp. 11–23.
[6] Liao, J., 2003, "Mechanical and Structural Properties of Mitral Valve Chordæ Tendineæ," Ph.D. thesis, Cleveland State University, Cleveland, Ohio.
[7] Trotter, J. A., Thurmond, F. A., and Koob, T. J., 1994, "Molecular Structure and Functional Morphology of Echinoderm Collagen Fibrils," Cell Tissue Res., **275**, pp. 451–458.
[8] Weiss, J. A., and Gardiner, J. C., 2001, "Computational Modeling of Ligament Mechanics," Crit. Rev. Biomed. Eng., **29**, pp. 303–371.
[9] Fratzl, P., Misof, K., Zizak, I., Rapp, G., Amenitsch, H., and Bernstorff, S., 1997, "Fibrillar Structure and Mechanical Properties of Collagen," J. Struct. Biol., **122**, pp. 119–122.
[10] Sasaki, N., and Odajima, S., 1996, "Elongation Mechanism of Collagen Fibrils and Force-Strain Relations of Tendon at Each Level of Structural Hierarchy," J. Biomech., **29**, pp. 1131–1136.
[11] Nauck, E. T., 1931, "Die Wellung der Sehnenfasern, ihre Ursache und ihre funktionelle Bedeutung," Gegenbaurs Morphol. Jahrb, **68**, pp. 79–96.
[12] Miyazaki, H., and Hayashi, K., 1999, "Tensile Tests of Collagen Fibers Obtained from the Rabbit Patellar Tendon," Biomed. Microdevices, **2**, pp. 151–157.
[13] Fung, Y.-C., 1967, "Elasticity of Soft Tissues in Simple Elongation," Am. J.

Physiol., **213**, pp. 1532–1544.
[14] Doehring, T. C., Carew, E. O., and Vesely, I., 2004, "The Effect of Strain Rate on the Viscoelastic Response of Aortic Valve Tissue: A Direct-Fit Approach," Ann. Biomed. Eng., **32**, pp. 223–232.
[15] Comninou, M., and Yannas, I. V., 1976, "Dependence of Stress-Strain Nonlinearity of Connective Tissues on the Geometry of Collagen Fibers," J. Biomech., **9**, pp. 427–433.
[16] Dale, W. C., Baer, E., Keller, A., and Kohn, R. R., 1972, "On the Ultrastructure of Mammalian Tendon," Experientia, **28**, pp. 1293–1295.
[17] Diamant, J., Keller, A., Baer, E., Litt, M., and Arridge, R. G. C., 1972, "Collagen; Ultrastructure and Its Relation to Mechanical Properties as a Function of Aging," Proc. R. Soc. London, Ser. B, **180**, pp. 293–315.
[18] Kastelic, J., Palley, I., and Baer, E., 1980, "A Structural Mechanical Model for Tendon Crimping," J. Biomech., **13**, pp. 887–893.
[19] Stouffer, D. C., Butler, D. L., and Hosny, D., 1985, "The Relationship Between Crimp Pattern and Mechanical Response of Human Patellar Tendon-Bone Units," ASME J. Biomech. Eng., **107**, pp. 158–165.
[20] Evans, J. H., and Barbenel, J. C., 1975, "Structure and Mechanical Properties of Tendon related to Function," Equine Vet. J., **7**, pp. 1–8.
[21] Yahia, L., and Drouin, G., 1989, "Microscopical Investigation of Canine Anterior Cruciate Ligament and Patellar Tendon: Collagen Fascicle Morphology and Architecture," J. Orthop. Res., **7**, pp. 243–251.
[22] Lerch, H., 1950, "Über den Aufbau des Schnengewebes," Gegenbaurs Morphol. Jahrb, **90**, pp. 192–205.
[23] Beskos, D. E., and Jenkins, J. T., 1975, "A Mechanical Model for Mammalian Tendon," ASME J. Appl. Mech., **42**, pp. 755–758.
[24] Lanir, Y., 1983, "Constitutive Equations for Fibrous Connective Tissues," J. Biomech., **16**, pp. 1–12.
[25] Ancker, C. J., Jr., and Goodier, J. N., 1958, "Theory of Pitch and Curvature Corrections for the Helical Springs—I (Tension)," ASME J. Appl. Mech., **25**, pp. 471–483.
[26] Belkoff, S. M., and Haut, R. C., 1991, "A Structural Model Used to Evaluate the Changing Microstructure of Maturing Rat Skin," J. Biomech., **24**, pp. 711–720.
[27] Rowe, R. W. D., 1985, "The Structure of Rat Tail Tendon Fascicles," Connect. Tissue Res., **14**, pp. 21–30.
[28] Millman, R. S., and Parker, G. D., 1977, *Elements of Differential Geometry*, Prentice-Hall, Englewood Cliffs, NJ.
[29] Langhaar, H. L., 1962, *Energy Methods in Applied Mechanics*, Wiley, New York.
[30] Seely, F. B., and Smith, J. O., 1952, *Advanced Mechanics of Materials*, 2nd ed., Wiley, New York.
[31] Carew, E. O., Doehring, T. C., Barber, J. E., Freed, A. D., and Vesely, I., 2003, "Fractional-Order Viscoelasticity Applied to Heart Valve Tissues," in: *Proceedings of the 2003 Summer Bioengineering Conference*, L. J. Soslowsky, T. C. Skalak, J. S. Wayne, and G. A. Livesay, eds., ASME, Key Biscayne, FL, pp. 721–722.
[32] Doehring, T. C., and Vesely, I. (unpublished).
[33] Hurschler, C., Loitz-Ramage, B., and Vanderby, R., Jr., 1997, "A Structurally Based Stress-Stretch Relationship for Tendon and Ligament," ASME J. Biomech. Eng., **119**, pp. 392–399.
[34] Sandor, B. I., 1978, *Strength of Materials*, Prentice-Hall, Englewood Cliffs, NJ.